ACTA PHYSIOLOGICA

Acta Physiol 2017, **219**, 441–452

Increased microvascular permeability in mice lacking Epac1 (Rapgef3)

R. K. Kopperud,[1,2,*,†] C. Brekke Rygh,[1,*,§] T. V. Karlsen,[1] C. Krakstad,[1] R. Kleppe,[1] E. A. Hoivik,[1,†] M. Bakke,[1] O. Tenstad,[1] F. Selheim,[1] Å. Lidén,[1,¶] L. Madsen,[1,3,‡] T. Pavlin,[1] T. Taxt,[1] K. Kristiansen,[3] F.-R. E. Curry,[4] R. K. Reed[1,2] and S. O. Døskeland[1]

1 Department of Biomedicine, University of Bergen, Bergen, Norway

2 Centre for Cancer Biomarkers (CCBIO), University of Bergen, Bergen, Norway

3 Department of Biology, University of Copenhagen, Copenhagen, Denmark

4 Department of Physiology and Membrane Biology, School of Medicine, University of California, Davis, CA, USA

Received 18 February 2016, revision requested 15 March 2016, revision received 12 April 2016, accepted 14 April 2016
Correspondence: S. O. Døskeland, MD, PhD, Jonas Lies vei 91, N-5009 Bergen, Norway. E-mail: stein.doskeland@uib.no

See Editorial Commentary: Waschke, J. Epac1 – a tonic stabilizer of the endothelial barrier. *Acta Physiol (Oxf)* **219**, 339–340.

*These authors contributed equally to this work.
†Present address: Department of Clinical Sciences, University of Bergen, Bergen, Norway
‡Present address: National Institute of Nutrition Research (NIFES), Bergen, Norway
§Present address: Bergen University College, Bergen, Norway
¶Present address: Galderma Nordic AB, Uppsala, Sweden

The copyright line for this article was changed on 11th August, 2016 after original online publication.

Abstract

Aim: Maintenance of the blood and extracellular volume requires tight control of endothelial macromolecule permeability, which is regulated by cAMP signalling. This study probes the role of the cAMP mediators rap guanine nucleotide exchange factor 3 and 4 (Epac1 and Epac2) for *in vivo* control of microvascular macromolecule permeability under basal conditions.

Methods: Epac1$^{-/-}$ and Epac2$^{-/-}$ C57BL/*6J* mice were produced and compared with wild-type mice for transvascular flux of radio-labelled albumin in skin, adipose tissue, intestine, heart and skeletal muscle. The transvascular leakage was also studied by dynamic contrast-enhanced magnetic resonance imaging (DCE-MRI) using the MRI contrast agent Gadomer-17 as probe.

Results: Epac1$^{-/-}$ mice had constitutively increased transvascular macromolecule transport, indicating Epac1-dependent restriction of baseline permeability. In addition, Epac1$^{-/-}$ mice showed little or no enhancement of vascular permeability in response to atrial natriuretic peptide (ANP), whether probed with labelled albumin or Gadomer-17. Epac2$^{-/-}$ and wild-type mice had similar basal and ANP-stimulated clearances. Ultrastructure analysis revealed that Epac1$^{-/-}$ microvascular interendothelial junctions had constitutively less junctional complex.

Conclusion: Epac1 exerts a tonic inhibition of *in vivo* basal microvascular permeability. The loss of this tonic action increases baseline permeability, presumably by reducing the interendothelial permeability resistance. Part of the action of ANP to increase permeability in wild-type microvessels may involve inhibition of the basal Epac1-dependent activity.

Keywords atrial natriuretic peptide, cAMP, endothelial junction, Epac deletion (mouse), microvascular permeability (*in vivo*), Rapgef.

The primary aim of the study was to investigate whether the cAMP-stimulated Rap activator Epac contributes to the tonic control of microvessel baseline permeability in major organs of the mouse. The well-recognized endothelial permeability lowering effect of cAMP was first thought to be mediated by cAMP-dependent protein kinase (PKA) only, but the likely involvement of Epac was demonstrated using Epac-activating cAMP analogues (Christensen *et al.*, 2003) that lowered the permeability of monolayers of human embryonic vascular endothelial cells and attenuated the response to inflammatory conditions such

as exposure to thrombin (Cullere *et al.* 2005). A role of Epac1 and its target, the small GTPase Rap, to modulate inflammation-associated endothelial hyperpermeability has been confirmed in numerous *in vitro* studies and noted in some *in situ* perfusion studies of accessible microvessels, although the relative roles of PKA, cGMP-dependent protein kinase (PKG) and Epac in different organ vascular beds and under different experimental conditions still remain uncertain (for recent reviews, see Spindler *et al.* 2010, Surapisitchat & Beavo 2011, Kuhn 2012, Curry & Adamson 2013).

The role of Epac to maintain stable baseline permeability in intact microvessels under non-inflammatory conditions is less well studied. A major reason is the lack of ways to reliably inhibit Epac and other cAMP-dependent pathways pharmacologically *in vivo* (Spindler & Waschke 2011), in part due to rapid metabolism and renal clearance of cAMP analogues used to modulate Epac and PKA activity (Kleppe *et al.* 2015).

In this study, Epac-deficient mice (Epac1$^{-/-}$ or Epac2$^{-/-}$) were generated to elucidate the potential *in vivo* role of Epac in regulation of baseline macromolecule flux across microvascular endothelium. Others have reported that Epac1$^{-/-}$ and Epac2$^{-/-}$ mice have only subtle phenotypes. Epac2$^{-/-}$ mice have a slightly perturbed pathway of pancreatic beta cell insulin exocytosis (Shibasaki *et al.* 2007), while Epac1$^{-/-}$ mice have been reported to gain slightly more (Kai *et al.* 2013) or slightly less (Yan *et al.* 2013) body weight on both low- and high-fat diets, and be less susceptible to rickettsial invasion (Gong *et al.* 2013).

We report here an increased basal microvascular transvascular albumin flux in skin, skeletal muscle and intestines of Epac1$^{-/-}$, but not Epac2$^{-/-}$ mice. Dynamic contrast-enhanced magnetic resonance imaging (DCE-MRI) studies of the masseter muscle using Gadomer-17 demonstrated transvascular flux of the high molecular weight MR contrast agent, which confirmed that Epac1$^{-/-}$ mice had constitutively increased microvascular permeability to macromolecules. Transmission electron microscopy was used to compare the ultrastructure of the endothelial junctions in masseter muscle biopsies from basal state in Wt and Epac1$^{-/-}$ mice. They revealed decrease of junctional complex in the interendothelial slits from Epac1$^{-/-}$ mice.

To evaluate further whether Epac1 and/or Epac2 contributed to the regulation of vascular permeability under physiological conditions, we tested the response of microvessels to the naturally circulating atrial natriuretic peptide (ANP) in Wt, Epac1$^{-/-}$ and Epac2$^{-/-}$mice. ANP is released when plasma volume is expanded and increases vascular permeability to albumin as part of the normal control of plasma volume. We and others have demonstrated this action in Wt mice (Curry *et al.* 2010, Lin *et al.* 2011), and also shown that it is attenuated when cAMP is elevated, and proposed that ANP might increase permeability via decreased Epac activity (Lin *et al.* 2011). We show here that Epac1-deficient mice, but not Epac2-deficient mice have an attenuated response to ANP.

Materials and methods

Ethical approval

The animal experiments were approved by the Norwegian Animal Research Authority and conducted according to the European Convention for the Protection of Vertebrates Used for Scientific Purposes, Norway.

Materials

The anti-Epac1 antibody was kindly provided by J. Bos, University of Utrecht, the Netherlands. The anti-Epac2 antibody (5B1) was from Cell Signaling technology (www.cellsignal.com). The anti-CD31 antibody (DIA-310) was from Dianova, Hamburg, Germany. ANP and rolipram were from Sigma-Aldrich (St. Louis, MO, USA). Gadomer-17 was from *in vivo* Contrast GmbH, Schering Pharma (Berlin, Germany). Human serum albumin (HSA) was labelled with ^{131}I or ^{125}I (from Perkin Elmer, Waltham, MA, USA) by the iodogen method, as previously described (Curry *et al.* 2010). Any free iodide was removed by spinning twice on a 3-kDa cut-off column (Microcon filter; Millipore, Bedford, MA, USA) prior to experiments. The labelled HSA eluted like native HSA upon anionic exchange and high-resolution size exclusion chromatography with online gamma radiation detection in series with UV detector. Low molecular weight radioactivity accounted for <0.3% of the total activity.

Generation of Epac1$^{-/-}$ and Epac2$^{-/-}$ knock-out models. Epac1$^{-/-}$ and Epac2$^{-/-}$ mice were generated by genomic deletion of exons 7–10 in *Rapgef3* (encoding Epac1) and exons 12–13 of *Rapgef4 (*encoding Epac2) encoding the cAMP-binding domains of both proteins (Fig. 1a,d) by use of the Cre–LoxP system. An additional frame shift codon was introduced in exon 11 in *Rapgef3* resulting in a stop codon at the start of exon 11 (Fig. 1a). Heterozygous floxed *Rapgef3* and *Rapgef4* mice were generated at the Mouse Clinical Institute, Strasbourg, France, and subsequently crossed with C57BL/6J mice expressing CRE recombinase from the CMV promoter resulting in global deletion of Epac1 and Epac 2 expression, as confirmed by immunoblotting and RT-PCR (Fig. 1b,c,e). C57BL/6JBomTac mice from Taconic, Denmark, were used to backcross the recombined chimeric mice for at least 10

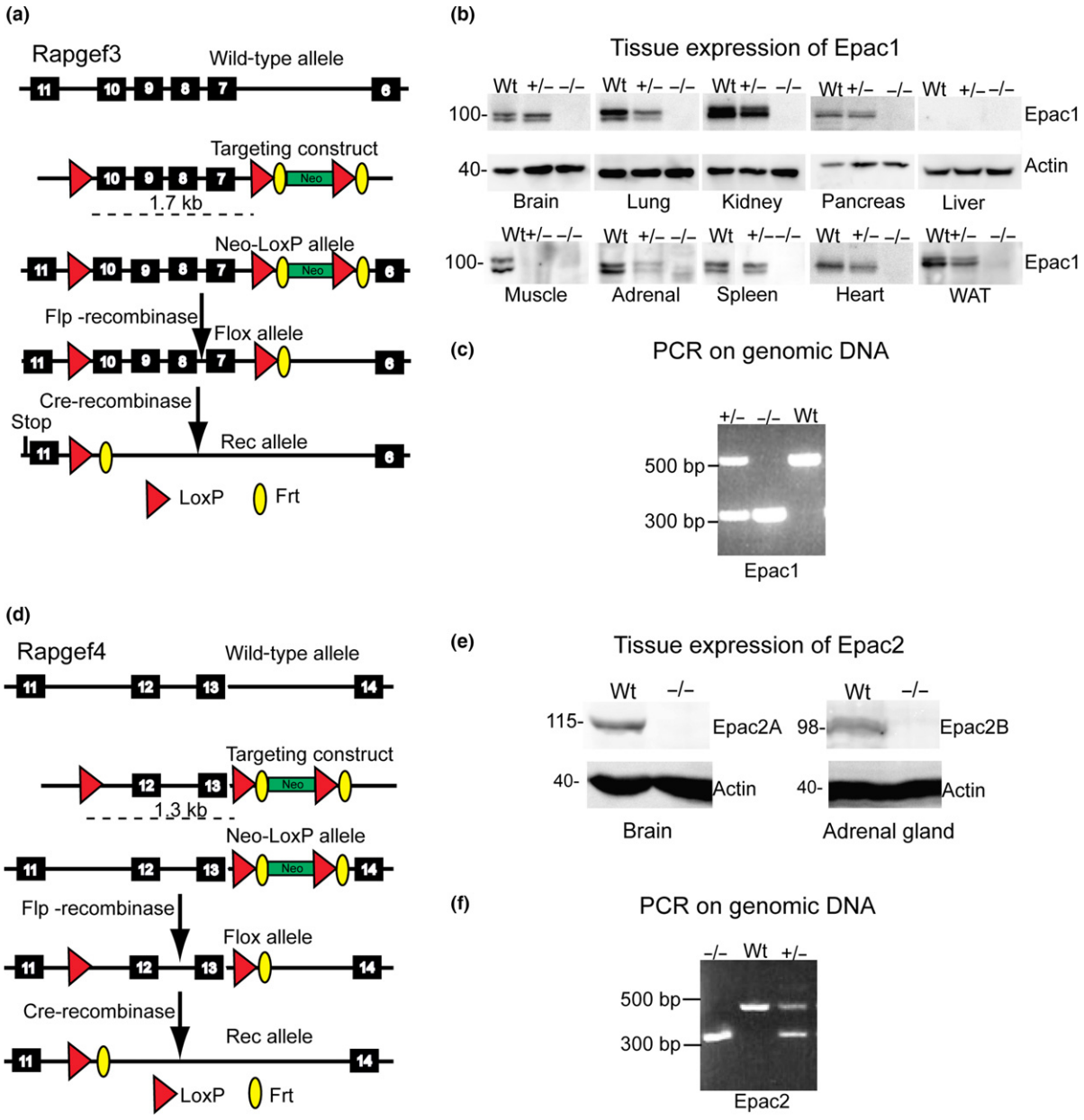

Figure 1 Generation of the Epac1$^{-/-}$ and Epac2$^{-/-}$ mouse strains. (a) The Epac1 (Rapgef3) gene targeting construct and deletion strategy. (b) Anti-Epac1 immunoblots showing lack of Epac1 protein in Epac1$^{-/-}$ mouse tissue and decreased expression in Epac1$^{-/+}$ compared to Wt tissue. (c) PCR genotyping demonstrates the sizes of PCR products predicted for the Epac1 deletion (see Methods for details; WAT is white adipose tissue). (d) The Epac2 (Rapgef4) gene targeting construct and the deletion strategy. The deletion includes the functional cAMP-binding domain common for all known Epac2 isoforms. (e) Anti-Epac2 immunoblots showing lack of Epac2 protein in Epac2$^{-/-}$ mouse organs (brain, adrenal cortex) with high expression of Epac2. (f) PCR genotyping validation of the deletion.

generations. The origin of the C57BL/6JBomTac mice is described at http://www.taconic.com/wmspage.cfm?parm1=764.

Genotyping

For genotyping, DNA was extracted from one 1.5-mm-diameter ear punch according to Truett *et al.* (2000). The deletion of exon 7–10 in Epac1$^{-/-}$and exon 12–13 in Epac2$^{-/-}$ was confirmed by PCR (Qiagen, Hilden, Germany; Multiplex PCR Kit, Cat.No: 206143) using primers P1–P3 and P4–P6 respectively.

P1, CAC-AGA-CAG-TGC-TTA-GCA-CAG-TGC; *P2*, CAC-CTC-TCT-TCC-CAA-ACC-TAG-AGC-C; *P3*, GCC-CCA-AGG-CTG-CTG-ATC-CC; *P4*, TGA-ATT-ATG-GGG-GAA-CGC-ACT-TTC-C; *P5*, GTG-TGG

-TGC-TAT-GAA-ATT-GGT-TCC-GTT-G; *P6*, TGC-C TC-CAT-TGT-TCT-TCG-GG.

The PCR was for 30 cycles of 94 °C (each 30 s), 63 °C (Epac1) or 60 °C (Epac2) for 90 s, 72 °C for 90 s, and finally 72 °C for 10 min. For Epac1, the predicted size of the <1000 bp PCR product is 525 bp for Wt and 315 bp for Epac1$^{-/-}$ tissue (P1–P3). For Epac2, it is 495 bp for Wt and 332 for Epac2$^{-/-}$ tissue (P4–P6).

Immuno (Western) blotting

Immunoblotting was performed essentially as described elsewhere (Gausdal *et al.* 2004). The membranes were probed with either mouse monoclonal anti-Epac1 or mouse monoclonal anti-Epac2. Bands representing the proteins of interest were detected using alkaline phosphatase-conjugated secondary antibodies and CDP-Star substrate (Tropix, Bedford, MA, USA) and band intensity determined in a Fuji LAS3000 (Fuji Photo Film, Tokyo, Japan).

Animal experiments

General. Artificial lighting was maintained on a 12 : 12-h light–dark cycle. Room temperature was kept constant at 23 °C, and the animals were provided with water and rodent chow *ad libitum*. The mice were 12–16 weeks old when used for experiments, the ratio of female to male mice being about one (0.8–1.2). The weight range was 20–25 g for the female and 25–30 g for the male mice. All experimental procedures were performed while animals were anesthetized using 3.5% isoflurane (Isoba vet; Schering-Plough Animal Health, Uxbridge, UK) and maintained with 1.5–2% isoflurane in air. The anaesthesia was supplied via a nose cone. During anaesthesia, the body temperature, and in the case of MRI, also the respiration rate was monitored continuously and kept stable during the experiments. A single catheter was placed in a tail vein (MRI) or the jugular vein (two-tracer method) for infusions.

Determination of arterial blood pressure. Arterial blood pressure (BP) was measured in five Epac1$^{-/-}$ and six wild-type mice by the tail-cuff method following the instructions of the manufacturer (CODA5; Kent Scientific, Torrington, CT, USA). Briefly, the mice were pre-warmed in an incubator at 32 °C for 30–45 min and then transferred to a tube for measuring the BP. The tubes were placed on a heating pad to keep the mice warm. The warming prevents tail vessel vasoconstriction and ensures optimal vasodilation for the blood pressure determination. Measurement of blood pressure was performed in five cycles, each 20 s. Each mouse was trained on day 1, and the blood pressure measured each of the two following days.

Determination plasma albumin and total protein concentration. Blood (20 μL) from the facial vein of live mice was drawn into syringes coated with acid–citrate–dextrose solution. The blood was centrifuged at 150 ***g*** for 4 min, and the resulting platelet-rich plasma centrifuged at 1000 ***g*** for another 5 min. The plasma concentration of albumin and total plasma protein was compared in Wt and Epac$^{-/-}$ mice using a label-free proteomic method as described elsewhere (Haslene-Hox *et al.* 2011).

The two-tracer method for determination of intact mouse tissue albumin clearance

The two-tracer method (Curry *et al.* 2010) was used to determine albumin clearance. The method depends on the sequential infusion of ^{125}I-HSA and ^{131}I-HSA. It has been validated for determination of albumin leakage in Wt mice and explained in detail in (Curry *et al.* 2010). In brief, ^{125}I-HSA (0.1 MBq) was given i.v. over 30 s in 0.05 mL of saline. Thirty minutes thereafter, ^{131}I-HSA (0.05 MBq) was injected (also i.v. in 0.05 mL of saline over 30 s). Five minutes thereafter, cardiac blood was withdrawn for plasma sampling, and the mice were killed by i.v. injection of saturated KCl. Tissue samples were rapidly dissected from back skin (four samples: left and right upper and lower quadrant), skeletal muscle (quadriceps), heart, small intestine (jejunum), large intestine (colon) and adipose tissue (inguinal white fat). The tissues and plasma samples were transferred to pre-weighed vials, which were sealed and immediately reweighed. After determination of radioactivity, the tissue samples were de-sealed and evaporated in a drying chamber at 60 °C. The vials were weighed repeatedly until stable weight (normally after 2–3 weeks) was reached. The radioactivity was determined in a gamma-counting system (LKB Wallac 1285, Turku, Finland). Spillover from ^{131}I to ^{125}I was corrected automatically. Blood-to-tissue clearance was estimated as the extravascular plasma equivalent volume of ^{125}I-HSA (counts min^{-1} per g dry tissue weight)/(counts min^{-1} per mL plasma). The clearance over 30 min is the difference between the plasma equivalent distribution volume of ^{125}I-HSA at 35 min and that of ^{131}I-HSA at 5 min. All clearances were referenced to tissue dry weight. The clearance data were also normalized to clearance per unit blood volume by dividing clearance by the plasma volume in the sample to minimize effects of variable blood filling between the samples (see Curry & Adamson 2010 for discussion).

DCE-MRI to determine Gadomer-17 microvascular clearance. Dynamic contrast-enhanced magnetic resonance imaging was performed to determine the clearance of macromolecular tracers. The MR contrast

agent Gadomer-17 has a molecular weight of 17 kDa, but due to its dendrimeric structure, its Stokes radius is as for globular proteins of molecular weight 35 kDa (Misselwitz *et al.* 2001). The contrast agent was injected over 15 s during scanning through a catheter in the tail vein after acquisition of 30 baseline images. For the ANP study, 0.4 mmol Gadomer kg^{-1} (diluted 1 : 4 in saline) was injected. In the rolipram study, 0.2 mmol Gadomer kg^{-1} was injected. The MRI was performed using a horizontal bore 7T small animal MRI instrument (PharmaScan; Bruker Corporation, Ettlingen, Germany), equipped with dedicated mouse bed and head coil. DCE-MRI data were obtained with a T1-weighted FLASH sequence (Fast Low Angle Shot) with a flip angle of 25°, repetition time and echo time of 13.77 and 2.52 ms respectively. A total of 600–1200 axial images through the masseter muscle were acquired with a sampling interval of 0.99 s, with a slice thickness of 1 mm, field of view of 2.5 cm and acquisition matrix of 96 × 96.

A separate group of animals ($n = 9$) was used to determine the signal over time in large supplying vessels to the head to estimate the arterial input function (AIF). An oblique sagittal slice was positioned over the carotid arteries, and 1200 T_1-weighted (same acquisition parameters as above) with a sampling interval of 0.99 s were acquired. The signal intensity over time was acquired in a region of interest of the internal masseter muscle using Nordic Image Control and Evaluation (nICE; Nordic Imaging Lab AS, Bergen, Norway). The data were further processed using MATLAB (The Mathworks, Natick, MA, USA) to implement the step/slope model as previously described (Curry *et al.* 2010). The rate constant (0.0063 s^{-1}) for Gadomer-17 was equal for all animals based on the estimation of the AIF above. The rate constants were estimated using blind deconvolution as previously described (Taxt *et al.* 2012).

Investigation of the effect of ANP and rolipram on Gadomer-17 clearance—Three series of experiments were performed. In the first series, 20 Epac1$^{-/-}$ and 20 Wt mice were used. Ten mice in each group received ANP and 10 received vehicle (PBS without potassium). ANP (500 ng (kg BW)$^{-1}$ min^{-1}) or vehicle was given as a 30 min continuous infusion before the Gadomer-17 injection. The DCE-MRI experiments were performed as described above. In the second series, 20 Epac2$^{-/-}$ and 20 Wt mice were used. Again, 10 mice in each group received ANP and 10 received vehicle. Finally, for the rolipram study, 20 Epac1$^{-/-}$ and 20 Wt mice were used. Ten of the mice in each group received 8 mg kg^{-1} BW rolipram intraperitoneally and 10 received vehicle just before the Gadomer-17 injection and start of MR image acquisition.

Investigation of the effect of ANP on albumin clearance—Atrial natriuretic peptide (500 ng (kg BW)$^{-1}$ min^{-1}) or vehicle was given as a continuous infusion for 30 min directly after the initial ^{125}I-HSA injection (as described above) to either 20 Epac1$^{-/-}$ or 20 Wt mice.

Transmission electron microscopy. Tissue was dissected from the mice immediately after euthanasia, sliced into 1 mm^3 cubes, fixed for 24 h in 1.5% glutaraldehyde in 0.1 M Na-cacodylate buffer (pH 7.4) and post-fixed in 1% osmium tetroxide (OsO_4) for 60 min. Dehydration was in graded alcohol solutions. After embedding in Agar 100 resin, ultra-thin sections were cut and stained with uranyl acetate and lead citrate. Sections were examined in a Jeol (Tokyo, Japan) JEM-1230 electron microscope. The sections were cut perpendicular to the long axis of the muscle fibres and their accompanying microvessels. The transverse microvessel sections were scrutinized for presence of endothelial slits (junctions), which were counted. High-magnification digital micrographs of the junctions were analysed on a screen for the presence and length of dense junctional complexes. In addition, the slit length (including any curvatures) and calibre (the interendothelial cell distance not obstructed by electron-dense material) was determined.

Immunohistochemical staining of endothelial CD31, estimation of capillary density. Sections (4 μm thick) of paraffin-embedded masseter muscle were dewaxed, microwave-treated with 10 mM citric acid, pH 6.0 and subsequently blocked for 10 min at 25 °C with 5% BSA and 5% normal rabbit serum in 0.05 M Tris, pH 7.4, 0.15 M NaCl (TBS) before being immunostained for 18 h with anti-CD31 antibody (1 : 20 in TBS with 1% BSA) at 4 °C. The sections were next treated with 3% H_2O_2 in PBS for 5 min before incubation with biotin-labelled secondary antibody (Biotinylated anti-rat IgG; Vector BA-4001) for 45 min. The immunohistochemical reactions were developed using the ABC Vectastain Elite staining kit (Vector Laboratories, Burlingame, CA, USA), based on avidin-coupled peroxidase. The sections were counterstained with haematoxylin. The number of capillaries per fibre was estimated based on counting 300–550 capillaries from 13 photographs of random sections from two Wt and two Epac1$^{-/-}$ mice.

Statistical methods

Differences between groups were tested with one-way ANOVA with subsequent post hoc testing using GRAPHPAD INSTAT (GraphPad Software, La Jolla, CA, USA). Two-tailed *t*-tests were used when comparing only two groups. When testing ANP-effects, one-tailed testing

was used as extensive studies by others and us have failed to demonstrate any case when ANP decreases endothelial permeability. The Mann–Whitney two-tailed *U*-test (http://elegans.som.vcu.edu/~leon/stats/utest.html) was used to assess whether endothelial slit calibre or the magnitude of endothelial junctional complex differed significantly between samples from Wt and Epac1$^{-/-}$ mice, as such data are not normally distributed. Values are generally given as mean ± SEM.

Results

Verification of the Epac deletions

The *Rapgef3* gene coding for Epac1 was silenced by a deletion comprising the exon coding for the cAMP-binding domain, removing the possibility of cAMP regulation of any product of the disrupted *Rapgef3* gene. The deletion introduced, in addition, a missense mutation to avoid translation of the C-terminal part active site containing part of the Epac1 molecule (see Fig. 1a for details). Epac1 was not detected by Western blot analysis in any tested tissue from the Epac1$^{-/-}$ mice. Compared with Wt mice, the expression was lower in Epac1$^{+/-}$ mice (Fig. 1b). The deletion was confirmed by PCR of genomic DNA (Fig. 1c).

A similar strategy (deletion of the functional cAMP-binding domain) was used for *Rapgef4* (Fig. 1d). The *Rapgef4* gene codes for 3 Epac2 size variants (a, b, c). Each variant has a separate promoter, whose methylation state decides which size variant is expressed (Ueno *et al.* 2001, Niimura *et al.* 2009, Hoivik *et al.* 2013). As the functional cAMP-binding domain is common for all size variants (Kawasaki *et al.* 1998, de Rooij *et al.* 1998), Epac2A (highly expressed in brain; Fig. 1e), Epac2B (highly expressed in adrenal cortex; Fig. 1e) and Epac2C (highly expressed in the parenchymal hepatocytes of the liver; not shown) were absent in the Epac2$^{-/-}$ mouse. PCR of genomic DNA confirmed the deletion of Epac2 (Fig. 1f). The Epac1$^{-/-}$ and Epac2$^{-/-}$ mice were able to reproduce and had normal life span.

Arterial blood pressure

The Epac1$^{-/-}$ mice have, like the Wt mice, normal blood pressure. After 2 days of habituation to the procedure, the mean arterial pressure in Wt mice was 101 ± 6.3 mmHg (systolic 122 ± 6.6 and diastolic 98 ± 6.4) against 102 ± 4.9 mmHg (124 ± 4.9 and 91 ± 5.2) in Epac1$^{-/-}$ mice. The first day after training, the mean pressure was slightly higher, but again near identical in Wt (108 ± 4.3) and Epac1$^{-/-}$ (108 ± 4.3) mice. We considered it therefore unlikely that the basal state microvascular transendothelial flux could differ in Wt and Epac1$^{-/-}$ mice due to divergent blood pressure.

Plasma albumin and total protein concentration

The albumin concentration and total plasma protein concentration were similar in Wt and Epac1$^{-/-}$ mice, as determined by quantitative proteomic analysis (arbitrary units). Serum albumin was 10.0 ± 1.0 and total protein 18.8 ± 0.8 in Wt, against 10.0 ± 0.2 and 17.8 ± 1.4 in Epac1$^{-/-}$ mice.

Epac1$^{-/-}$ mice have constitutively increased microvascular albumin permeability in major organs

The movement of albumin from the vascular to the extravascular compartment was evaluated by the two-tracer method. The experiments were executed in two separate series (one for Epac1$^{-/-}$ and one for Epac2$^{-/-}$), each with Wt animals as control. The two Wt groups were tested against each other. As there was no difference between them, a combined group consisting of all Wt animals was used for comparison with the Epac1$^{-/-}$ and Epac2$^{-/-}$ animals.

The local plasma volume of each tissue sample was determined from the content of ^{131}I-HSA, which was infused 5 min before euthanasia, and was similar in tissue samples from Wt, Epac1$^{-/-}$ and Epac2$^{-/-}$ animals (for details see legend to Fig. 2). The Epac1$^{-/-}$ mice had significantly increased albumin clearance (normalized to plasma volume) in skin, skeletal muscle, adipose tissue and large intestine (Fig. 2). An increase in albumin clearance when expressed relative to local plasma volume is a strong indication of an actual change in vascular permeability, as it compensates for differences in surface area for exchange. In contrast to Epac1$^{-/-}$ mice, the Epac2$^{-/-}$ mice had albumin clearance similar to Wt mice in skin, skeletal muscle, adipose tissue and large intestine, but was increased in the small intestine (Fig. 2). Taken together, these results indicate that Epac1, but not Epac2, provided a significant contribution to the basal macromolecular endothelial permeability in most of the organs studied here.

The microvascular clearance of the MRI contrast agent Gadomer-17 is enhanced in the masseter muscle of Epac1$^{-/-}$ mice

To obtain further evidence for a role of Epac1 in macromolecule endothelial permeability and eliminate the (unlikely) possibility that increased albumin clearances were due to an albumin-specific uptake mechanism, additional studies were performed using the

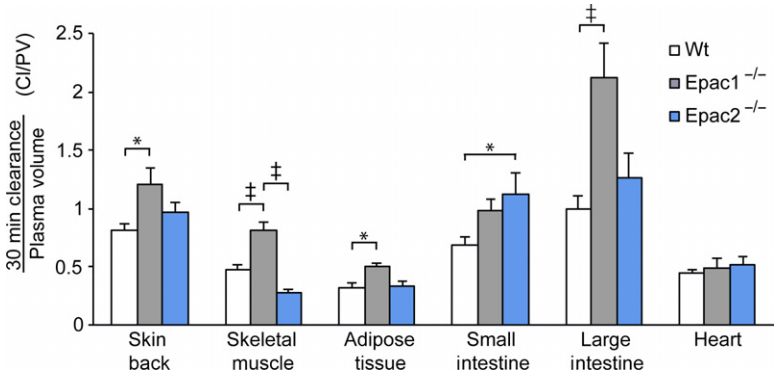

Figure 2 The normalized albumin clearance is increased in skin, skeletal muscle, adipose tissue and large intestine of Epac1$^{-/-}$, but not Epac2$^{-/-}$ mice. The normalized clearance (NC) in tissue samples of back skin, skeletal muscle, white adipose tissue, small and large intestine, and heart is shown mL g^{-1} dry weight (average ± SEM). The NC is the ratio of the clearance (based on relative tissue sample content of ^{125}I-HSA infused 35 min before euthanasia) and the local tissue plasma volume (relative content of ^{131}I-HSA, infused 5 min before euthanasia). *P*-values < 0.05 (*) and <0.001 (±) are shown. The plasma volume (mL g^{-1} dry weight) was, with the exception of jejunum from the Epac2$^{-/-}$ mice, similar between Wt (n = 19), Epac1$^{-/-}$ (n = 9) and Epac2$^{-/-}$ (n = 9) mouse tissues: Skin: Wt: 0.023 ± 0.002, Epac1$^{-/-}$: 0.020 ± 0.002, Epac2$^{-/-}$: 0.027 ± 0.003; quadriceps muscle (corresponding values): 0.022 ± 0.003, 0.014 ± 0.001, and 0.018 ± 0.002; inguinal fat: 0.024 ± 0.001, 0.023 ± 0.002 and 0.028 ± 0.003; jejunum: 0.101 ± 0.008, 0.116 ± 0.017 and 0.064 ± 0.006; colon: 0.042 ± 0.004, 0.033 ± 0.002 and 0.032 ± 0.003; heart: 0.229 ± 0.013, 0.215 ± 0.019, and 0.205 ± 0.015. HSA, human serum albumin.

synthetic macromolecule Gadomer-17 in the immobilized M. masseter skeletal muscle of Wt and Epac1$^{-/-}$ mice. The initial rapid rise of the MRI signal after intravenous Gadomer-17 injection seen in Figure 3a reflected blood vessel filling and was similar for Wt and Epac1$^{-/-}$ animals, suggesting near-identical vascular volumes. Thereafter, the MR signal intensity became higher in muscle from Epac1$^{-/-}$ mice than Wt mice, indicating increased constitutive permeability in Epac1$^{-/-}$ microvasculature. Apparently, the loss of Epac1 affected a pathway for microvascular macromolecule exchange common for albumin and Gadomer-17 (Fig. 3b). We finally tested whether lack of Epac1 also could blunt the known permeability decreasing effect of the cAMP elevating PDE4 inhibitor rolipram in the masseter muscle (Lin *et al.* 2011). Rolipram induced a lowering of Gadomer-17 permeability that was blunted in Epac1$^{-/-}$ masseter

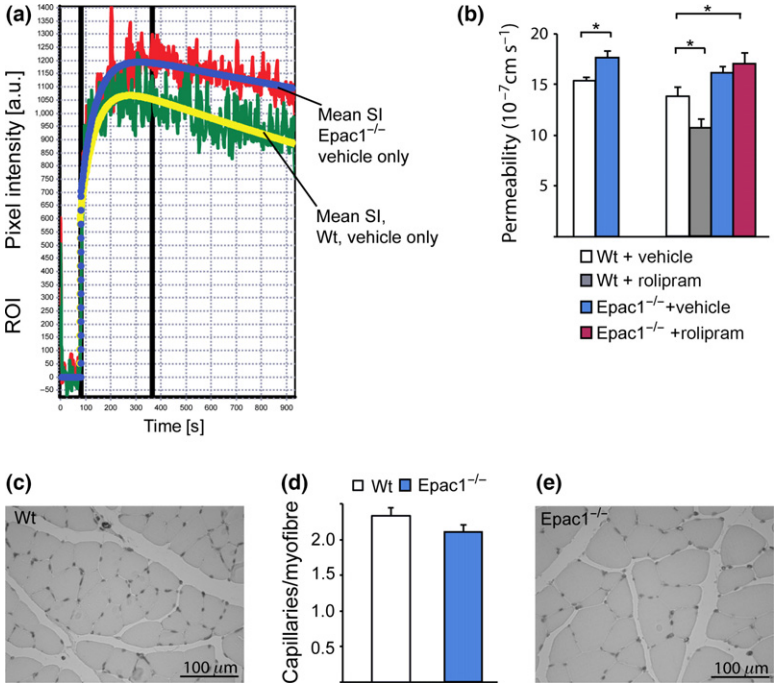

Figure 3 The constitutive Gadomer-17 clearance is increased in masseter muscle of Epac1$^{-/-}$ compared to Wt mice. (a) Typical magnetic resonance imaging (MRI) signal intensity (SI) obtained upon continuous scanning of a masseter region from Epac1$^{-/-}$ (red) or Wt (green) mouse before and after Gadomer (Gd)-17 injection. The solid lines show fits based on the calculated permeability coefficient. (b) The Gd 17 permeability coefficient calculated from the scanning data obtained before and after infusion of vehicle or rolipram, each animal serving as its own control. *P*-values < 0.05 are shown (n = 10). (c–e) The endothelium of transverse sections of M. masseter from Epac1$^{-/-}$ (c) or Wt (e) mice was visualized by anti-CD31 staining and the capillary/myofibre ratio determined (d). Error bars are SEM. *P*-values < 0.05 (*) are shown.

(Fig. 3b). The results could not be explained by decreased microvascularity in the Epac1$^{-/-}$ masseter as its capillary density was similar to Wt masseter (Fig. 3c–e). We conclude that Epac1$^{-/-}$ masseter has increased microvascular permeability both under basal and rolipram-stimulated conditions.

Comparison of the microvascular permeability enhancing effect of ANP in Wt and Epac1$^{-/-}$ mice

We and others have previously demonstrated that ANP increases the baseline microvascular permeability of Wt mice, particularly in skin and muscle (therefore, one-tailed *t*-testing was used). It is not known whether ANP acts through Epac1 inhibition or independently of Epac1. We reasoned that if ANP acted independently of Epac or an Epac-induced pathway, it should enhance permeability to the same level in Wt and Epac1$^{-/-}$ mice. We failed to note any further ANP-induced increase of permeability in the Epac1$^{-/-}$ mice (Fig. 4a,b), unlike in the Epac2$^{-/-}$ mice (Fig. 4c). Besides, the albumin permeability enhancing effect of ANP was, if anything, slightly lower in magnitude than the effect of deleting Epac1 (Fig. 4a). The above results are consistent with an action of ANP to reduce the effectiveness of an Epac1 pathway to maintain the constitutive vascular permeability.

A possible consequence of constitutively increased loss of albumin from the vascular to the extravascular compartment could be a slight increase of interstitial oncotic pressure accompanied by a slight water accumulation. As the tissue samples to be analysed for albumin isotope content were weighed before and after drying (see the Experimental section for details), we could compare their water content (relative to dry weight). Only in skin was the water content high enough to produce experimentally reliable data. Epac1$^{-/-}$ back skin had about 2% higher water content than back skin from Wt mice (Fig. 5). Further, the magnitude of the increase in water content was similar whether or not they were treated with ANP. This is not unexpected due to the short exposure time to ANP and the modest albumin permeability rate of back skin under the experimental conditions. In contrast, the Epac1$^{-/-}$ mice have a constitutive opportunity to retain fluid subsequent to the increased albumin permeability.

Epac1$^{-/-}$ microvessels have structurally less constricted interendothelial slits

We next studied whether the different Gadomer-17 permeability observed between Wt and Epac1$^{-/-}$ masseter muscle had structural microvascular correlates.

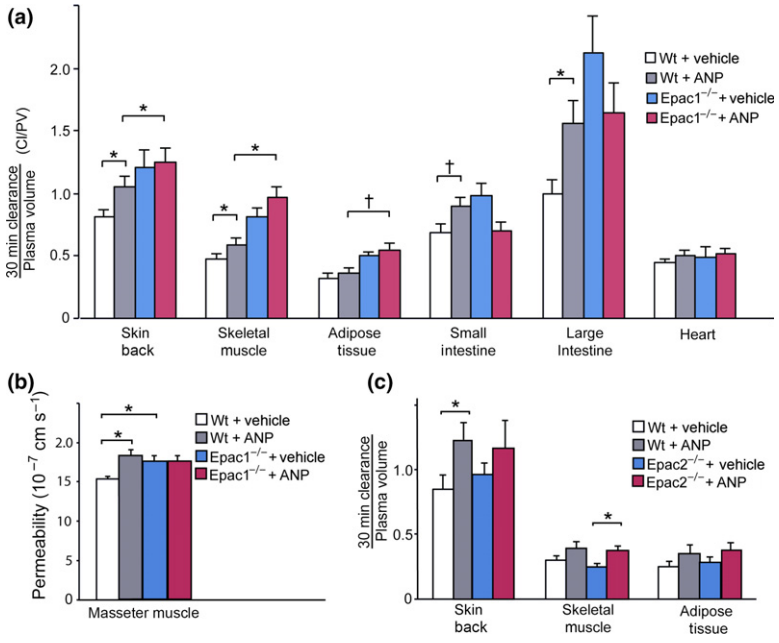

Figure 4 The effect of atrial natriuretic peptide (ANP) on macromolecule microvascular permeability in tissue from Wt, Epac1$^{-/-}$ and Epac2$^{-/-}$ mice. (a) The effect of ANP on the normalized albumin clearance is shown for tissues from Wt and Epac1$^{-/-}$ mice. The mice were given vehicle or ANP 30 minutes before euthanasia, and the apparent plasma volume and albumin clearance determined by the [^{131}I]albumin/[^{125}I]albumin method as for the experiment shown in Figure 2. (b) The effect of ANP on the microvascular permeability of Gadomer-17 is shown for masseter muscle from Wt and Epac1$^{-/-}$ mice. (c) The effect of ANP on the normalized albumin clearance for tissues from Wt and Epac2$^{-/-}$ mice. Error bars are SEM (n = 10). *P*-values < 0.05 (*) and <0.01 (+) are shown.

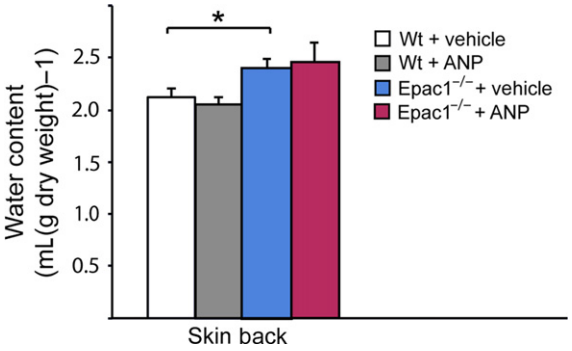

Figure 5 The water content of back skin from Wt and Epac1$^{-/-}$ mice. The water content (mL g^{-1} dry weight) of back skin from Epac1$^{-/-}$ mice and Wt mice injected with vehicle or atrial natriuretic peptide (ANP) was determined in the tissue samples used for the experiments on albumin clearance shown in Figures 2 and 4a, as described in the experimental section. Error bars are SEM (n = 10). P-value < 0.05 (*) is shown.

As already noted, the microvessel density did not differ between Epac1$^{-/-}$ and Wt masseter muscle (Fig. 3c–e). We therefore investigated transverse sections of Epac1$^{-/-}$ masseter muscle microvessels by electron microscopy for differences at the ultrastructural level. These analyses revealed a trend towards shorter and wider junctions in Epac1$^{-/-}$ capillaries (average length and width were 395 and 13 nm in Epac1$^{-/-}$ against 483 and 11 in Wt; P > 0.05). More importantly, a highly significant difference existed between Wt and Epac1$^{-/-}$ endothelial slits regarding the extent and density of junctional complex material. On average, Wt clefts had 224 nm of strongly developed junctional complex against only 97 nm for Epac1$^{-/-}$ clefts (Fig. 6a). Four of the 48 slit sections scrutinized from Epac1$^{-/-}$ microvessels had no constrictions <6 nm and no areas with strong accumulation of junctional complex material, against only one for the 57 studied slits from Wt mice. The most extreme examples of slit difference in distribution of electron-dense material are shown in Figure 6b–e. These observations demonstrated ultrastructural differences between endothelial slits from Wt and Epac1$^{-/-}$ animals under basal conditions, consistent with the finding that macromolecules such as Gadomer-17 and albumin have increased capillary permeability in Epac1$^{-/-}$ compared with Wt tissues.

Discussion

The present study demonstrates increased albumin clearance in several tissues of Epac1$^{-/-}$ mice under basal *in vivo* conditions. The Epac1$^{-/-}$ animals have normal plasma protein levels, normal blood pressure, and similar microvessel density and initial tissue blood filling of injected labelled albumin or Gadomer-17 as Wt animals. Enhanced transendothelial vesicle transport of surface receptor bound albumin has been described in some ANP-stimulated specialized endothelia (Chen *et al.* 2012), but is unlikely to

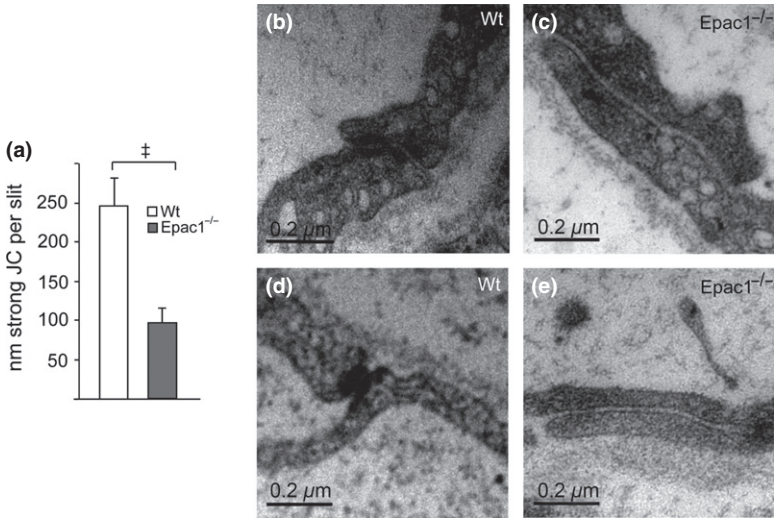

Figure 6 The endothelial junctional density of Epac1$^{-/-}$ and Wt capillaries. (a) The average length of each endothelial slit found associated with strong junctional complex (JC) in Wt and Epac1$^{-/-}$ M. masseter. Error bars are SEM. The P-value for the difference between Epac1$^{-/-}$ and Wt slits was <0.00002 by the Mann–Whitney two-tailed U-test and <0.0003 by the two-tailed t-test. (b–e) Examples of junctions from Wt and Epac1$^{-/-}$ mice. The two Wt junctions shown (b, c) had more abundant JC than found in any of the 48 Epac1$^{-/-}$ junctions studied. The two Epac1$^{-/-}$ junctions shown (d, e) had less abundant JC than any of 57 Wt junctions studied.

explain the enhanced albumin clearance of Epac1$^{-/-}$ animals as they had increased clearance also of the artificial macromolecule Gadomer-17. Our results therefore conform to the hypothesis that tonic activity of Epac1-dependent pathways contributes to the maintenance of baseline vascular permeability, and loss of this activity leads to a sustained increase in baseline permeability. We ascribe this phenotype to enhanced permeability of the interendothelial junctions of Epac1$^{-/-}$ mouse microvessels.

A number of studies implicate PKA alone or PKA and Epac together as responsible for cAMP-induced endothelial barrier tightening (Rampersad *et al.* 2010, Surapisitchat & Beavo 2011, Curry & Adamson 2013). The present study does not exclude an action of PKA in maintaining the endothelial barrier *in vivo*, but suggests that Epac1 has a dominant role compared to PKA in intact microvessels as treatment with rolipram, which would increase cAMP and PKA activity, failed to overcome the lack of Epac1 (Fig. 3). A similar dominant role of Epac1 was noted in arterial endothelial cells *in vitro*, where the junctional protein VE-cadherin colocalizes with PKA, a PDE4D/Epac1 complex, and the Epac target Rap1 in a 'signalosome' controlling the paracellular permeability (Rampersad *et al.* 2010). It is noted that these conclusions apply principally to the situation where the molecular complexes regulating cAMP are tethered close to the cell membrane. The tethering of PKA, Epac1 and their substrates close to sites of production of cAMP or cGMP and members of the cyclic nucleotide phoshodiesterase (PDE) family of cyclic nucleotide degrading enzymes is an important part of the regulatory scheme (Maurice 2011). Thus, lung endothelial cells responded to cAMP produced by a soluble bacterial adenylyl cyclase by interendothelial cell gap formation, facilitating bacterial invasion and oedema formation. The same cells showed restricted permeability, however, when cAMP was produced close to the surface membrane. In either case, the cAMP effect was attributed to PKA activation (Prasain *et al.* 2009, Ochoa *et al.* 2012).

Our observations provide new insight into mechanisms that regulate vascular permeability. In particular, they imply that Epac1 activity exerts a tonic inhibition of microvessel permeability. One potential way to relieve the Epac1-dependent inhibition in the intact animal is by lowering the cAMP concentration close to the endothelial junction. In fact, this has been proposed as explanation for the ANP-enhanced microvessel permeability. The ability of ANP to enhance microvascular albumin clearance depends on its binding to the endothelial cGMP producing receptor GC-A (Kuhn *et al.* 2009, Kuhn 2012). The resulting cGMP increase can (i) directly activate PKG, (ii) directly inhibit PDE3 degradation of cAMP and thus indirectly activate PKA and Epac, or (iii) directly activate PDE2 to indirectly lower cAMP and thereby reduce PKA and Epac activity (Surapisitchat *et al.* 2007, Birukova *et al.* 2008, Kuhn 2012). Epac1 does not bind cGMP at physiologically relevant concentrations (Christensen *et al.* 2003), but as in (iii) above, a cGMP burst can inhibit Epac indirectly by stimulating PDE2 to degrade cAMP in an endothelial cell compartment close to Epac1 (Kraynik *et al.* 2013). This scenario is compatible with the present findings as the ANP effect was blunted or absent in the Epac1$^{-/-}$ animals (Fig. 4a) and that rolipram, a strong inhibitor of the cAMP-specific PDE4, easily overrides ANP-induced hyperpermeability *in vivo* (Lin *et al.* 2011). Such overriding is less easily explained for purely cGMP-regulated putative ANP mediators like PKG (Schreier *et al.* 2008). Besides, the constitutive endothelial barrier resistance was lowered to at least a similar extent by Epac1 deficiency compared to exposure to ANP, as expected if ANP acted to inhibit Epac1 through a moderate decrease of endothelial cell cAMP (Kraynik *et al.* 2013).

As our animal models had global Epac deletion, the observed endothelial phenotype might in part be caused by deletion of Epac1 in non-endothelial cells. We considered therefore whether it could be related to constitutively increased aldosterone output from the adrenal cortex, where ANP decreases aldosterone production through GC-A/cGMP/PDE2-dependent lowering of cAMP (Tsai & Beavo 2011). This is unlikely because the adrenocortical cells express Epac2 rather than Epac1 (Niimura *et al.* 2009, Hoivik *et al.* 2013, see also Fig. 1e), and our Epac2$^{-/-}$ animals responded fully to ANP (Fig. 4c). Secondly, the ANP effect on microvascular permeability is abolished in mice with endothelial-specific deletion of the GC-A receptor for ANP (Curry *et al.* 2010). Thirdly, our Epac mice had normal blood pressure, arguing that their renin–angiotensin–aldosterone axis was unperturbed. The present study supports therefore the notion that ANP may modulate endothelial permeability *in vivo* through lowering the cAMP concentration near Epac1.

The ultrastructural analysis of the junctions between endothelial microvessel cells demonstrated less electron-dense junction complex material in Epac1$^{-/-}$ than in Wt microvessels (Fig. 6). Thus, it is likely that microvessels in Epac1$^{-/-}$ mice have more discontinuities in the band of tight junction material that effectively seals the junctions to molecules the size of albumin and Gadomer-17. The effect of such discontinuities on permeability depends on their three-dimensional arrangement (Weinbaum & Curry 1995, Michel & Curry 1999). Assuming a similar arrangement in wt and Epac1$^{-/-}$ mice, our results are consistent with a hyperpermeable state. The present study does not

address whether the paucity of junction material in Epac1$^{-/-}$ slits is readily reversible, but it may be noted that the forskolin/rolipram-induced endothelial barrier tightening of rat mesenteric post-capillary venules occurs rapidly *in vivo* (Spindler *et al.* 2011).

An important question is the role of Epac1-dependent pathways in relation to other signal mediators, such as sphingosine-1 phosphate (S1P) that also exerts a tonic control of vascular permeability (Curry & Adamson 2013). As it is reasonable to assume that S1P was present at normal levels in our experiments, we conclude that reduced Epac1 activity can increase permeability at physiological levels of S1P.

Our observations have potentially useful translational implications. Agents selectively targeting Epac1 may be sufficient and more precise tools than general cAMP agonists to modulate the endothelial barrier *in vivo*. Cyclic nucleotide analogues, including those with potential as Epac1 modulators, so far have not been useful in intact mammals, mainly because they, like cAMP itself, are rapidly cleared through active renal excretion and metabolism by phosphodiesterases (for recent review see Kleppe *et al.* 2015). New inhibitors of Epac that act outside the cyclic nucleotide binding site have been produced. So far, they are specific for Epac2 (Tsalkova *et al.* 2012, Chen *et al.* 2013), which appears not to be involved in the control of the endothelial barrier. Nevertheless, this new inhibitor class indicates a route to produce modulators of Epac1, which may become useful to control the endothelial barrier.

Conflict of interest

The authors declare that they have no conflicts of interest.

Gerd Salvesen, Trude Skogstrand, Bodil Hansen, Reidar Myklebust, Anne Nyhaug, Nina Lied Larsen and Ingeborg Brønstad provided expert technical assistance. All MRI and TEM experiments were performed at the Molecular Imaging Center (MIC) at the University of Bergen, Norway. Funding was from the Research Council of Norway (NRC), The Western Norway Health Authority (WNRH) and the Norwegian Cancer Association (DNK). FEC was supported by NIH grant HL028607-32.

References

Birukova, A.A., Zagranichnaya, T., Alekseeva, E., Bokoch, G.M. & Birukov, K.G. 2008. Epac/Rap and PKA are novel mechanisms of ANP-induced Rac-mediated pulmonary endothelial barrier protection. *J Cell Physiol* **215**, 715–724.

Chen, W., Gassner, B., Borner, S., Nikolaev, V.O., Schlegel, N., Waschke, J., Steinbronn, N., Strasser, R. & Kuhn, M. 2012. Atrial natriuretic peptide enhances microvascular albumin permeability by the caveolae-mediated transcellular pathway. *Cardiovasc Res* **93**, 141–151.

Chen, H., Ding, C., Wild, C., Liu, H., Wang, T., White, M.A., Cheng, X. & Zhou, J. 2013. Efficient synthesis of ESI-09, a novel non-cyclic nucleotide EPAC antagonist. *Tetrahedron Lett* **54**, 1546–1549.

Christensen, A.E., Selheim, F., de Rooij, J., Dremier, S., Schwede, F., Dao, K.K., Martinez, A., Maenhaut, C., Bos, J.L., Genieser, H.G. & Doskeland, S.O. 2003. cAMP analog mapping of Epac1 and cAMP kinase. Discriminating analogs demonstrate that Epac and cAMP kinase act synergistically to promote PC-12 cell neurite extension. *J Biol Chem* **278**, 35394–35402.

Cullere, X., Shaw, S.K., Andersson, L., Hirahashi, J., Luscinskas, F.W. & Mayadas, T.N. 2005. Regulation of vascular endothelial barrier function by Epac, a cAMP-activated exchange factor for Rap GTPase. *Blood* **105**, 1950–1955.

Curry, F.R. & Adamson, R.H. 2010. Vascular permeability modulation at the cell, microvessel, or whole organ level: towards closing gaps in our knowledge. *Cardiovasc Res* **87**, 218–229.

Curry, F.R. & Adamson, R.H. 2013. Tonic regulation of vascular permeability. *Acta Physiol (Oxf)* **207**, 628–649.

Curry, F.R., Rygh, C.B., Karlsen, T., Wiig, H., Adamson, R.H., Clark, J.F., Lin, Y.C., Gassner, B., Thorsen, F., Moen, I., Tenstad, O., Kuhn, M. & Reed, R.K. 2010. Atrial natriuretic peptide modulation of albumin clearance and contrast agent permeability in mouse skeletal muscle and skin: role in regulation of plasma volume. *J Physiol* **588**, 325–339.

Gausdal, G., Gjertsen, B.T., Fladmark, K.E., Demol, H., Vandekerckhove, J. & Doskeland, S.O. 2004. Caspase-dependent, geldanamycin-enhanced cleavage of co-chaperone p23 in leukemic apoptosis. *Leukemia* **18**, 1989–1996.

Gong, B., Shelite, T., Mei, F.C., Ha, T., Hu, Y., Xu, G., Chang, Q., Wakamiya, M., Ksiazek, T.G., Boor, P.J., Bouyer, D.H., Popov, V.L., Chen, J., Walker, D.H. & Cheng, X. 2013. Exchange protein directly activated by cAMP plays a critical role in bacterial invasion during fatal rickettsioses. *Proc Natl Acad Sci USA* **110**, 19615–19620.

Haslene-Hox, H., Oveland, E., Berg, K.C., Kolmannskog, O., Woie, K., Salvesen, H.B., Tenstad, O. & Wiig, H. 2011. A new method for isolation of interstitial fluid from human solid tumors applied to proteomic analysis of ovarian carcinoma tissue. *PLoS ONE* **6**, e19217.

Hoivik, E.A., Witsoe, S.L., Bergheim, I.R., Xu, Y., Jakobsson, I., Tengholm, A., Doskeland, S.O. & Bakke, M. 2013. DNA methylation of alternative promoters directs tissue specific expression of Epac2 isoforms. *PLoS ONE* **8**, e67925.

Kai, A.K., Lam, A.K., Chen, Y., Tai, A.C., Zhang, X., Lai, A.K., Yeung, P.K., Tam, S., Wang, J., Lam, K.S., Vanhoutte, P.M., Bos, J.L., Chung, S.S., Xu, A. & Chung, S.K. 2013. Exchange protein activated by cAMP 1 (Epac1)-deficient mice develop beta-cell dysfunction and metabolic syndrome. *FASEB J* **27**, 4122–4135.

Kawasaki, H., Springett, G.M., Mochizuki, N., Toki, S., Nakaya, M., Matsuda, M., Housman, D.E. & Graybiel, A.M. 1998. A family of cAMP-binding proteins that directly activate Rap1. *Science* **282**, 2275–2279.

Kleppe, R., Madsen, L., Herfindal, L., Selheim, F. & Døskeland, S.O. 2015. Assessing cyclic nucleotide recognition in

cells: opportunities and pitfalls for selective receptor activation. Chapter 4. In: X. Cheng (ed.) *CRC Series on Methods in Signal Transduction*, Vol. Title "*Cyclic Nucleotide Signaling*", pp. 61–80. CRC Press, Taylor & Francis, Boca Raton, FL, London, New York, NY. ISBN 1482235560

Kraynik, S.M., Miyaoka, R.S. & Beavo, J.A. 2013. PDE3 and PDE4 isozyme selective inhibitors are both required for synergistic activation of brown adipose tissue. *Mol Pharmacol* **83**, 1155–1166.

Kuhn, M. 2012. Endothelial actions of atrial and B-type natriuretic peptides. *Br J Pharmacol* **166**, 522–531.

Kuhn, M., Volker, K., Schwarz, K., Carbajo-Lozoya, J., Flogel, U., Jacoby, C., Stypmann, J., van Eickels, M., Gambaryan, S., Hartmann, M., Werner, M., Wieland, T., Schrader, J. & Baba, H.A. 2009. The natriuretic peptide/guanylyl cyclase–a system functions as a stress-responsive regulator of angiogenesis in mice. *J Clin Invest* **119**, 2019–2030.

Lin, Y.C., Samardzic, H., Adamson, R.H., Renkin, E.M., Clark, J.F., Reed, R.K. & Curry, F.R. 2011. Phosphodiesterase 4 inhibition attenuates atrial natriuretic peptide-induced vascular hyperpermeability and loss of plasma volume. *J Physiol* **589**, 341–353.

Maurice, D.H. 2011. Subcellular signaling in the endothelium: cyclic nucleotides take their place. *Curr Opin Pharmacol* **11**, 656–664.

Michel, C.C. & Curry, F.E. 1999. Microvascular permeability. *Physiol Rev* **79**, 703–761.

Misselwitz, B., Schmitt-Willich, H., Ebert, W., Frenzel, T. & Weinmann, H.J. 2001. Pharmacokinetics of Gadomer-17, a new dendritic magnetic resonance contrast agent. *MAGMA* **12**, 128–134.

Niimura, M., Miki, T., Shibasaki, T., Fujimoto, W., Iwanaga, T. & Seino, S. 2009. Critical role of the N-terminal cyclic AMP-binding domain of Epac2 in its subcellular localization and function. *J Cell Physiol* **219**, 652–658.

Ochoa, C.D., Alexeyev, M., Pastukh, V., Balczon, R. & Stevens, T. 2012. Pseudomonas aeruginosa exotoxin Y is a promiscuous cyclase that increases endothelial tau phosphorylation and permeability. *J Biol Chem* **287**, 25407–25418.

Prasain, N., Alexeyev, M., Balczon, R. & Stevens, T. 2009. Soluble adenylyl cyclase-dependent microtubule disassembly reveals a novel mechanism of endothelial cell retraction. *Am J Physiol Lung Cell Mol Physiol* **297**, L73–L83.

Rampersad, S.N., Ovens, J.D., Huston, E., Umana, M.B., Wilson, L.S., Netherton, S.J., Lynch, M.J., Baillie, G.S., Houslay, M.D. & Maurice, D.H. 2010. Cyclic AMP phosphodiesterase 4D (PDE4D) Tethers EPAC1 in a vascular endothelial cadherin (VE-Cad)-based signaling complex and controls cAMP-mediated vascular permeability. *J Biol Chem* **285**, 33614–33622.

de Rooij, J., Zwartkruis, F.J., Verheijen, M.H., Cool, R.H., Nijman, S.M., Wittinghofer, A. & Bos, J.L. 1998. Epac is a Rap1 guanine-nucleotide-exchange factor directly activated by cyclic AMP. *Nature* **396**, 474–477.

Schreier, B., Borner, S., Volker, K., Gambaryan, S., Schafer, S.C., Kuhlencordt, P., Gassner, B. & Kuhn, M. 2008. The heart communicates with the endothelium through the guanylyl cyclase-A receptor: acute handling of intravascular volume in response to volume expansion. *Endocrinology* **149**, 4193–4199.

Shibasaki, T., Takahashi, H., Miki, T., Sunaga, Y., Matsumura, K., Yamanaka, M., Zhang, C., Tamamoto, A., Satoh, T., Miyazaki, J. & Seino, S. 2007. Essential role of Epac2/Rap1 signaling in regulation of insulin granule dynamics by cAMP. *Proc Natl Acad Sci USA* **104**, 19333–19338.

Spindler, V. & Waschke, J. 2011. Beta-adrenergic stimulation contributes to maintenance of endothelial barrier functions under baseline conditions. *Microcirculation* **18**, 118–127.

Spindler, V., Schlegel, N. & Waschke, J. 2010. Role of GTPases in control of microvascular permeability. *Cardiovasc Res* **87**, 243–253.

Spindler, V., Peter, D., Harms, G.S., Asan, E. & Waschke, J. 2011. Ultrastructural analysis reverals cAMP-dependent enhancement of microvascular endothelial barrier functions via Rac1-mediated reorganization of intercellular junctions. *Am J Pathol* **178**, 2424–2436.

Surapisitchat, J. & Beavo, J.A. 2011. Regulation of endothelial barrier function by cyclic nucleotides: the role of phosphodiesterases. *Handb Exp Pharmacol* **204**, 193–210.

Surapisitchat, J., Jeon, K.I., Yan, C. & Beavo, J.A. 2007. Differential regulation of endothelial cell permeability by cGMP via phosphodiesterases 2 and 3. *Circ Res* **101**, 811–818.

Taxt, T., Jirik, R., Rygh, C.B., Gruner, R., Bartos, M., Andersen, E., Curry, F.R. & Reed, R.K. 2012. Single-channel blind estimation of arterial input function and tissue impulse response in DCE-MRI. *IEEE Trans Biomed Eng* **59**, 1012–1021.

Truett, G.E., Heeger, P., Mynatt, R.L., Truett, A.A., Walker, J.A. & Warman, M.L. 2000. Preparation of PCR-quality mouse genomic DNA with hot sodium hydroxide and tris (HotSHOT). *Biotechniques* **29**, 52, 54.

Tsai, L.-C.L. & Beavo, J.A. 2011. The roles of cyclic nucleotide phosphodiesterases (PDE's) in steroidogenesis. *Curr Opin Pharmacol* **11**, 670–675.

Tsalkova, T., Mei, F.C., Li, S., Chepurny, O.G., Leech, C.A., Liu, T., Holz, G.G., Woods, V.L. Jr & Cheng, X. 2012. Isoform-specific antagonists of exchange proteins directly activated by cAMP. *Proc Natl Acad Sci USA* **109**, 18613–18618.

Ueno, H., Shibasaki, T., Iwanaga, T., Takahashi, K., Yokoyama, Y., Liu, L.M., Yokoi, N., Ozaki, N., Matsukura, S., Yano, H. & Seino, S. 2001. Characterization of the gene EPAC2: structure, chromosomal localization, tissue expression, and identification of the liver-specific isoform. *Genomics* **78**, 91–98.

Weinbaum, S. & Curry, F.E. 1995. Modelling the structural pathways for transcapillary exchange. *Symp Soc Exp Biol* **49**, 323–345.

Yan, J., Mei, F.C., Cheng, H., Lao, D.H., Hu, Y., Wei, J., Patrikeev, I., Hao, D., Stutz, S.J., Dineley, K.T., Motamedi, M., Hommel, J.D., Cunningham, K.A., Chen, J. & Cheng, X. 2013. Enhanced leptin sensitivity, reduced adiposity, and improved glucose homeostasis in mice lacking exchange protein directly activated by cyclic AMP isoform 1. *Mol Cell Biol* **33**, 918–926.